Ab initio simulation of the equation of state and kinetics of shocked water

Nir Goldman, Evan J. Reed, I.-F. William Kuo, Laurence E. Fried, Christopher J. Mundy, and Alessandro Curioni

Citation: The Journal of Chemical Physics **130**, 124517 (2009); doi: 10.1063/1.3089426
View online: http://dx.doi.org/10.1063/1.3089426
View Table of Contents: http://scitation.aip.org/content/aip/journal/jcp/130/12?ver=pdfcov
Published by the AIP Publishing

Ab initio simulation of the equation of state and kinetics of shocked water

Nir Goldman,[1,a)] Evan J. Reed,[1] I.-F. William Kuo,[1] Laurence E. Fried,[1] Christopher J. Mundy,[2] and Alessandro Curioni[3]
[1]*Physical and Life Sciences Directorate, Lawrence Livermore National Laboratory, Livermore, California 94550, USA*
[2]*Chemical and Materials Science Division, Pacific Northwest National Laboratory, Richland, Washington 99352, USA*
[3]*IBM Research, Zurich Research Laboratory, CH-8803 Ruesschlikon, Switzerland*

(Received 29 October 2008; accepted 6 February 2009; published online 30 March 2009)

We report herein first principles simulations of water under shock loading and the chemical reactivity under these hot, compressed conditions. Using a recently developed simulation technique for shock compression, we observe that water achieves chemical equilibrium in less than 2 ps for all shock conditions studied. We make comparison to the experimental results for the Hugoniot pressure and density final states. Our simulations show that decomposition occurs through the reversible reaction $H_2O \leftrightarrow H^+ + OH^-$, in agreement with experiment. Near the approximate intersection of the Hugoniot and the Neptune isentrope, we observe high concentrations of charged species that contribute electronic states near the band gap. © *2009 American Institute of Physics*. [DOI: 10.1063/1.3089426]

I. INTRODUCTION

Studies on water under extreme conditions are particularly relevant to planetary interiors, where the high conductivities within the predominantly water layers of Neptune and Uranus could generate planetary magnetic fields at relatively shallow depths.[1] Despite being an area of intense research, the high pressure-temperature properties of water are still relatively unknown. Diamond anvil cell experiments have successfully accessed high pressure, low temperature states of water,[2,3] as well as the lower pressure, high temperature melting line of compressed ices.[4–7] Thermodynamic states that have been inaccessible with diamond anvil cells have traditionally been achieved through shock compression. Shock compression dynamically strains the sample in one spatial dimension while simultaneously heating the sample.[8] Shock induced melting[9–11] and freezing[12,13] of H_2O ices have been studied at relatively low pressures (approximately 5 GPa), and laser driven shock compression studies on liquid water have been conducted up to 790 GPa.[14] However, shock compression experiments can rely on equation of state models for temperatures, which have been shown to overestimate measured temperatures for water above 3000 K by approximately 17%.[15] In addition, the time to establish chemical equilibrium in shocked condensed matter is not well understood, with most studies to date occurring on organic[16] and/or explosive materials.[17,18] Disagreement also exists between theoretical and experimental studies regarding the chemical mechanism for ionic transport in shock compressed water. Shock compression experiments on water have suggested that charge transport occurs through classical diffusion of H^+ ions, created through a unimolecular dissociation mechanism, $H_2O \rightarrow OH^- + H^+$.[19,20] In contrast, it has been predicted in off-Hugoniot (not shocked) simulations[21] that proton hopping occurs between hydronium ions (H_3O^+), produced through a bimolecular dissociation mechanism similar to ambient water, $2H_2O \rightarrow OH^- + H_3O^+$. Thus, experiments could benefit from accurate molecular dynamics (MD) simulations along the shock Hugoniot for both equation of state data and elucidation of results.

Until recently, obtaining a clear theoretical picture of the chemistry behind shock fronts has been exceedingly difficult due to the extremely large system sizes required for such simulations.[22] Empirical potentials[17] and tight-binding simulations[16] have been used successfully to simulate the shock compression of several reactive systems. However, accurate modeling of the breaking and forming of chemical bonds in MD simulations frequently requires the use of quantum theories such as density functional theory (DFT), e.g., Ref. 23. DFT has been shown to accurately reproduce the high pressure-temperature phase boundaries of water,[7,24] as well as spectroscopic signatures of high pressure ices through different phase transitions.[25,26] Regardless, DFT-MD simulations are limited to system sizes of tens to hundreds of particles due to the extreme computational cost. This precludes a direct one-to-one simulation of shock compression experiments. Indirect simulation of the shock Hugoniot through large numbers (e.g., >60) of small constant volume simulations[27] is computationally prohibitive for most systems and excludes any nonequilibrium kinetic effects or metastable states that occur during shock compression.[28] Thus, a computational capability to access both electronic states and information on chemical bonding while accurately capturing the manifold of thermodynamic states present in a shock is necessary to elucidate chemical processes at extreme pressures and temperatures.

To circumvent the above scaling issues we use the multiscale shock technique (MSST).[18,28–31] MSST is a simulation methodology based on the Navier–Stokes equations for

a)Electronic mail: goldman14@llnl.gov.

compressible flow. Instead of simulating a shock wave within a large computational cell with many atoms,[22] the MSST computational cell follows a Lagrangian point through the shock wave as if the shock were passing over it. This is accomplished by time-evolving equations of motion for the atoms and volume of the computational of cell to constrain the stress in the propagation direction $\sigma_{xx} \equiv p$ to the Rayleigh line and the energy of the system to the Hugoniot energy condition.[29–31] In the case of a shock, conservation of mass, momentum, and energy across the shock front leads to the Hugoniot relation $E-E_0=\frac{1}{2}(P+P_0)(V_0-V)$, where E is the energy, P is the negative of the diagonal component of the stress tensor in the direction of the shock, and V is the volume. A subscript 0 refers to the preshocked state, while quantities without subscripts refer to the postshocked state. The Rayleigh line $P-P_0=U^2\rho_0(1-\rho_0/\rho)$ (where U is the shock velocity and ρ is the density) describes the thermodynamic path connecting the initial state of the system to its final (Hugoniot) state. For a given shock speed, these two relations describe a steady planar shock wave within continuum theory. By constraining the MD system to obey these relations, MSST enables simulation of the shock wave with significantly fewer atoms and consequently with significantly smaller computational cost. MSST has been shown to accurately reproduce the sequence of thermodynamic states throughout the reaction zone of shock compressed explosives with analytical equations of state.[31] Linear scaling of computational work with simulation duration has enabled simulation lengths of up to 0.2 ns of tight-binding *ab initio* MD simulations of shock compressed nitromethane.[18]

In this work we report DFT-MD simulations of the shock Hugoniot of water, using MSST in conjunction with Born–Oppenheimer MD in the CPMD software package.[32] We show that our calculated Hugoniot densities, pressures, and temperatures compare well to experiment, providing excellent validation of DFT at these extreme conditions. We then analyze the chemical species and lifetimes present in water under these extreme conditions. Our computed ionic conductivities accurately reproduce the experimental high pressure plateau, which we determine is caused by a unimolecular decomposition mechanism. Finally, we find that the presence of short-lived negatively charged species contributes to band gap closure at the highest pressure investigated in our study.

II. COMPUTATIONAL DETAILS

We performed simulations of the following shock velocities (km/s): 5, 6.5, 7.5, 9, 10, and 11. Stronger shock velocities resulted in electronic excitation beyond the Born–Oppenheimer state, which was beyond the scope of the current study. For all simulations, a planewave cutoff of 120 Ry was used with the Becke–Lee–Yang–Parr exchange-correlation functional.[33,34] Tests with the Perdew-Burke-Ernzerhof exchange-correlation functional[35] yielded consistent results over the pressure-temperature range of our calculations. An initial configuration of 64 H_2O molecules was generated from an equilibrated CPMD simulation conducted at 300 K with computational-cell lattice vectors of $a=19.72$ Å, $b=9.86$ Å, and $c=9.86$ Å. This corresponds to the ambient density of 1 g/cm^3, similar to initial conditions of experiments.[20] Uniaxial compression of the shock wave occurred along the a lattice vector. Convergence tests with up to 128 molecules showed that a system size of 32 molecules provided sufficient convergence of the stress tensor for the shock compressed configurations. A fictitious box mass of 3.5×10^6 a.u. and a wave function convergence criteria of 10^{-6} a.u. were used for all simulations. Simulations at 10 and 11 km/s had an additional force convergence criteria of 10^{-7} a.u. All simulations were between 5 and 11 ps in length. The average drift from the Hugoniot energy condition was less than 0.5% for the highest shock velocity simulated. Molecular species were identified with a bond distance and lifetime criteria discussed below.

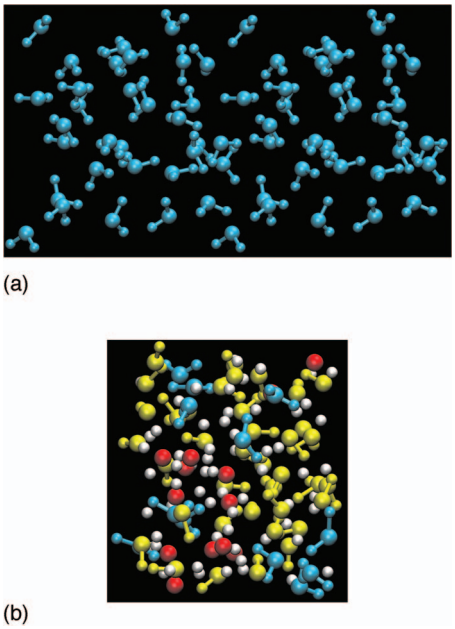

FIG. 1. (Color) Snapshots of the computational cell during shock compression at 11 km/s. The smaller size of (b) is due to the shock compression of the cell. H_2O molecules and bonds are colored blue, OH are yellow, unbonded O ions are red, and unbonded H are white. Very few H_3O^+ species were observed at this shock velocity.

III. RESULTS

In general, a constant hot, dense thermodynamic state was achieved in our simulations within 1 ps or less. Following this compression, simulations were observed to rapidly transform to an ensemble of short-lived H_2O molecules and various ions (H^+, OH^-, and O^{2-}) (Fig. 1). H_3O^+ ions were observed upon initial compression for some simulations, but decreased in concentration as the system equilibrated. At 6.5 km/s, chemical equilibrium was observed 2–3 ps after shock compression. At 9 km/s, the time to equilibration dropped to approximately 1 ps (Fig. 2). Atomic oxygen was observed to form approximately 500 fs after the first OH species at this shock velocity. At a shock velocity of 11 km/s, the system achieved chemical equilibrium in 250 fs after shock compression. The extremely short time scale is surprising given the measurement of much slower (nanoseconds) times to equilibration in shocked high explosives at roughly similar P, T conditions.[18,36]

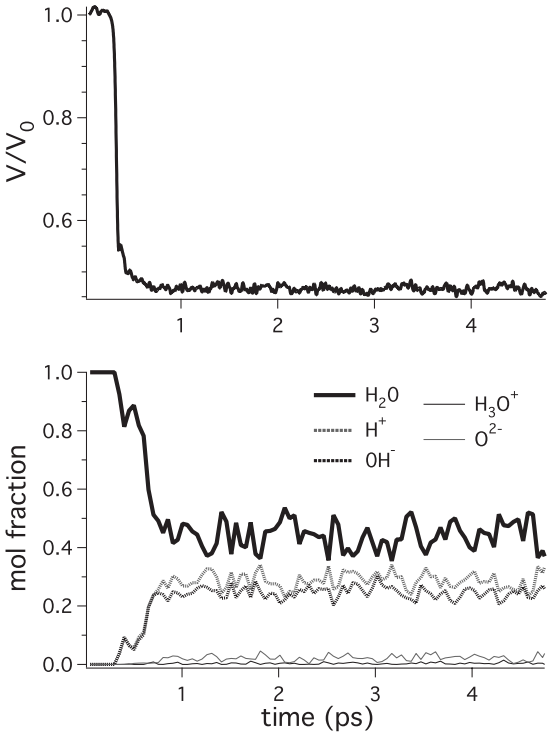

FIG. 2. Time dependence of the relative cell volume (top) and mole fraction (bottom) of chemical species during shock compression to 42.0 GPa (9 km/s). Equilibrium is achieved within approximately 1 ps. Concentration values were averaged over 50 fs increments.

Our results for the shock Hugoniot of water are shown in Figs. 3 and 4 and Table I. Our simulations provide quantitative validation of the DFT-generalized gradient approximation equation of state over a wide range of pressures (approximately 8–68 GPa). The error in the density is much lower than that at ambient conditions,[40] most likely because of the decreased importance of van der Waals interactions at extreme conditions. We find that our calculated temperatures agree well with experiment (Fig. 4). Comparison between calculated and experimental shock Hugoniot temperatures is

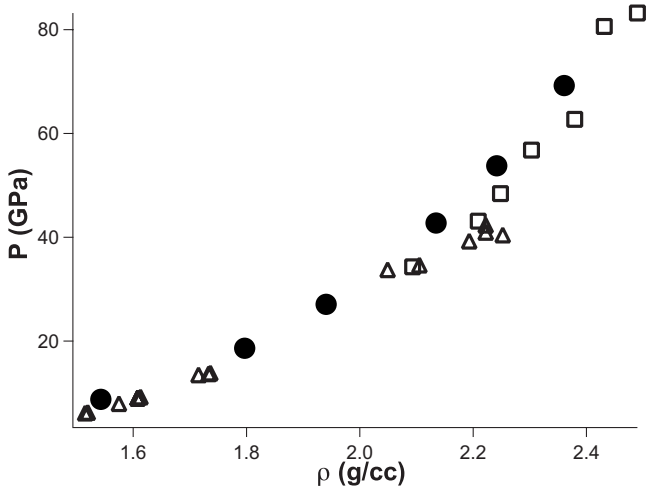

FIG. 3. Plot of pressure vs density Hugoniot results. Our simulation results are shown with the solid black circles, the open triangles are experimental results from Walsh *et al.* (Ref. 37), and the open squares are experimental results from Mitchell and Nellis (Ref. 38).

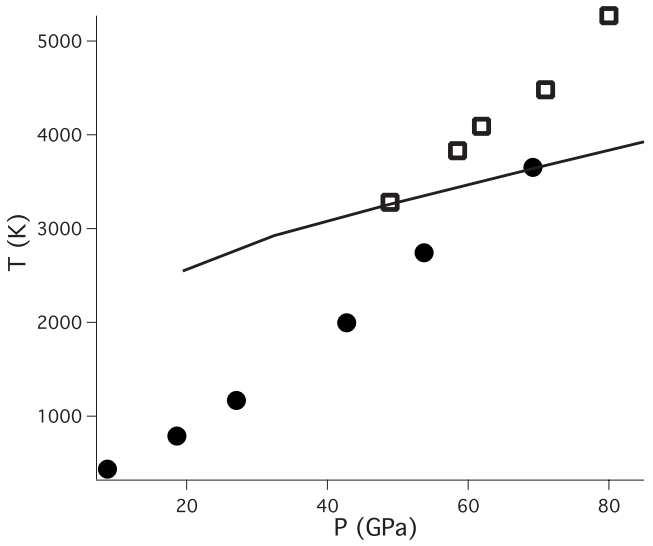

FIG. 4. Plot of the temperature vs pressure Hugoniot results. The solid black circles correspond to our *ab initio* MD results, and the open squares to experimental results from Lyzenga *et al.* (Ref. 15). The solid line corresponds to the Neptune isentrope (Ref. 39), digitally scanned from Ref. 1.

difficult considering that experimental pyrometric measurements are known to have extremely large uncertainties[1] due to difficulties in measuring emissivities from samples. Simultaneously, MD simulations have been shown to underpredict experimental temperatures by up to 20%–30%,[27] partially due to the exclusion of nuclear quantum vibrational effects in standard MD simulations.

We now analyze the chemical species prevalent in water at these conditions. Previous calculations have used both instantaneous electronic and geometric bond definitions in their simulations.[21] In the electronic definition, maximally localized Wannier functions[41] were used to determine the number of O–H covalent bonds in which each oxygen atom participates, whereas in the geometric definition, each hydrogen is assigned to be bonded to the nearest oxygen atom. Both of these criteria do not take into account the transient nature of chemical bonds at high pressures and temperatures, and the geometric definition precludes observation of free H atoms. Similar to previous work,[42–44] in our simulations we define molecular species by first choosing an optimal bonding cutoff r_c for all O–H bonds. The optimal value for r_c to distinguish between bonded and nonbonded atomic sites is given by the first minimum in the O–H radial distribution function, which corresponds to the maximum of the potential

TABLE I. Table of final thermodynamic states for our shock compression simulations. Error bars were determined by calculating the standard deviation over four time blocks.

Shock velocity (km/s)	Temperature (K)	Pressure (GPa)	Density (g/cm^3)
5	434 ± 14	8.3 ± 0.1	1.54 ± 0.01
6.5	791 ± 7	18.2 ± 0.2	1.80 ± 0.01
7.5	1167 ± 4	26.5 ± 0.4	1.94 ± 0.01
9	1995 ± 8	42.0 ± 0.3	2.13 ± 0.01
10	2744 ± 10	53.8 ± 0.3	2.24 ± 0.01
11	3654 ± 6	67.8 ± 0.2	2.36 ± 0.01

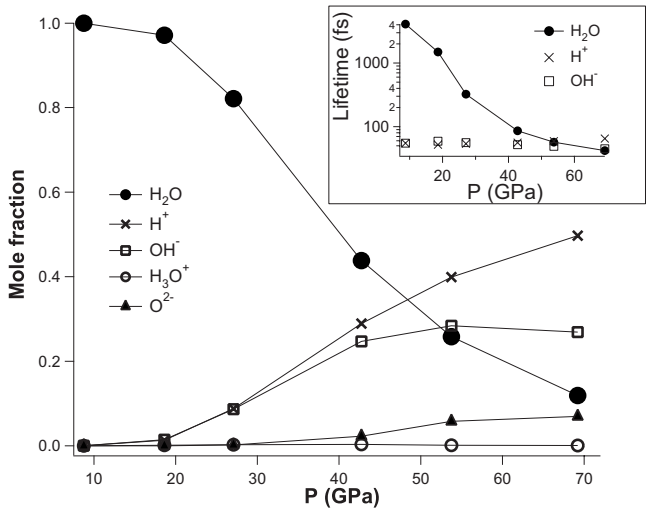

FIG. 5. Species concentrations as a function of pressure. As the simulations achieve higher pressure, there is a larger degree of ionization. Inset: Calculated molecular lifetimes of H_2O, OH^-, and H^+. Shorter lived species (viz. H_3O^+ and O^{2-}) are left out for the sake of clarity.

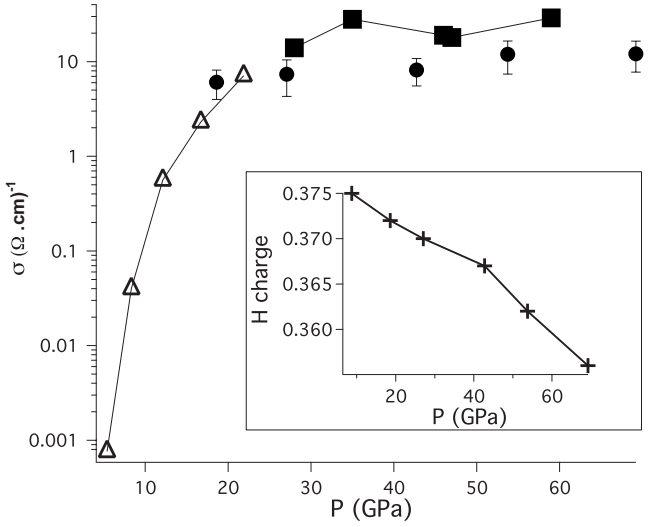

FIG. 6. Results for the ionic conductivity of water under shock compression. The open triangles correspond to experimental results from Hamann and Linton (Ref. 51), the solid squares to experiments from Mitchell and Nellis (Ref. 38), and the solid circles to our results. Error bars were determined by calculating the standard deviation in x, y, and z directions. Results for simulations at 5 km/s have been omitted due to the extremely large error bars associated with the small number of ionization events. Inset: Mulliken charges calculated for hydrogen.

of mean force, viz., $W(R_{OH})=-k_BT\ln[g(R_{OH})]$. This choice corresponds to the minimum in the reactive flux for dissociation, which is the optimal definition of the transition state within transition state theory.[45] We have chosen a value of $r_c=1.2$ Å for all of our simulations. In addition, in order to avoid counting species that were entirely transient and not chemically bonded,[43] we also chose a lifetime cutoff of 20 fs (e.g., two oscillations of an O–H bond vibration). This criteria are intuitive since O–H bonds with this lifetime could conceivably be detected spectroscopically. As a result, atom pairs were considered to be bonded only if they resided within a distance of each other of r_c for a time of greater than 20 fs. Using these bonding criteria, specific molecular species were then defined by recursively creating a data tree of all atomic bonds branching from the original bonded pair. The chemical reactivity, concentrations, and lifetimes of different species were then determined by monitoring the creation and dissociation of specific molecules during the course of the simulations.

The results for the species concentrations and lifetimes are shown in Fig. 5. Ions such as H, O, OH, and H_3O are reported with their formal charges for the sake of clarity. Unless otherwise noted, averaging over 1 ps time blocks did not produce any discernible change in the calculated lifetimes and concentrations. We have systematically tracked all chemical reactions in our simulations. At 8.3 GPa (5 km/s) we predict mostly H_2O molecules with lifetimes on the order of several picoseconds. We largely observe reversible unimolecular dissociation of H_2O into H^+ and OH^- pairs at 18.2 GPa (6.5 km/s), although trace amounts of H_3O^+ were present for several picoseconds after shock compression. As we compress further to 42.0 GPa (9 km/s), we observe chemical equilibration within 1 ps after compression. At this pressure the lifetimes and concentrations of H_2O, H^+, and OH^- are all roughly equivalent (approximately 50–90 fs). At this point it becomes difficult to describe water as having molecular species since the calculated lifetimes were all roughly equal to the chosen cutoff. Increasing the bond lifetime criteria to $\geq$50 fs at this pressure removed all indications of H_3O^+ and decreased the mole fraction of H_2O from 0.5 to $<$0.25. As the simulations were further compressed to 67.8 GPa (11 km/s), we observe subpicosecond equilibration to H^+, O^{2-}, and OH^-, where the lifetimes of all species are vanishingly small (approximately 20–30 fs). Analysis of the chemical reactivity for all simulations revealed that upon equilibration virtually none of the water decomposition occurs via dissociation of H_2O into H_3O^+ and OH^- pairs. A unimolecular dissociation mechanism of $H_2O \rightarrow OH^- + H^+$ dominates with our bond distance cutoff even when the bond lifetime cutoff is removed. We note that use of the same instantaneous geometric bonding cutoff as in Ref. 21 at 26.5 GPa (7.5 km/s) yielded similar mole fractions for H_3O^+ and OH^- at similar conditions to those in Ref. 21.

We have calculated the ionic conductivity using the relation $\sigma=(F^2/RTV)\int_0^\infty dt\langle \mathbf{J}(0)\cdot\mathbf{J}(t)\rangle$,[46] where F is Faraday's constant, R is the universal gas constant, T is temperature, and V is the cell volume. $\mathbf{J}(t)=\Sigma_j q_j \mathbf{v}_j(t)$ is the charge flux for all particles, where q_j and $\mathbf{v}_j$ are the charge and velocity of the jth particle, respectively. For each shock velocity we first calculated the average Mulliken charge[47,48] on all oxygens and hydrogens for 30 different MD snapshots spaced throughout the simulation. The small variation in charge (5%–15%) at each Hugoniot point allowed us to take $q_j(t)=\langle q_j(t)\rangle \equiv q_j$, which reduced the number of computationally expensive wave function evaluations required. Use of this autocorrelation function circumvents previously discussed difficulty in differentiating between transient ions and free ions that contribute to conduction.[49,50] Figure 6 shows excellent agreement between our results and experiments,[38,51] particularly at higher pressures. The conductivities calculated here along the shock Hugoniot are similar to those inferred on the basis of H^+ diffusion constants by Cavazzoni *et al.*[52]

along the planetary isentrope of Neptune. Our results also reproduce the experimentally measured plateau in conductivity, starting at approximately 30 GPa. We can conclude that this plateau over the conditions of our simulations is due to the transient nature of covalent bonds at these conditions, in which all species are more or less ionized.[20] As a result, no more ionic carriers can be produced, and the ionic conductivity occurs through classical diffusion of the protons. Calculations of the electronic component of the conductivity of high pressure-temperature water[53] indicate that there could be an onset of electronic conductivity at 67.8 GPa, the highest pressure investigated in our study. However, experimental studies show that in shock compressed water the electronic contribution to the conductivity is not significant until well above 180 GPa and 5000 K.[14]

We have calculated the electronic band gap of shocked water for all of our simulations.[48] At 8.3 GPa (5 km/s) we calculate a gap of 4.7 eV, which shrinks to 2.1 eV at 67.8 GPa (11 km/s). The reduction in the band gap as a function of pressure has been calculated previously (e.g., Ref. 53). At 67.8 GPa we determine a small number of configurations with near gap closure (<0.1 eV). This behavior was not seen in any of our simulations at lower pressure conditions. We have used Wannier functions to calculated a projected electron density of states[54] (DOS) for 20 of such configurations in order to determine which chemical species are contributing occupied states near the band gap. The vast majority of the near gap states are due to negatively charged OH and O, with OH having the most significant contribution (approximately 60%). Interestingly, H_2O species contribute a small percentage (approximately 8%) to the DOS near the Fermi energy due to H_2O molecules with near linear geometries. In order to investigate electron finite temperature effects on the band gap at these conditions, we have calculated a 10 ps long simulation of 64 H_2O at 2.45 g/cm^3 and 4000 K (close to the Hugoniot state at 11 km/s) with Fermi smearing of the electronic occupancies,[55] using identical simulation parameters (PBE exchange-correlation functional[35] and 900 eV planewave cutoff) to Ref. 53. We observe that the band gap oscillates between approximately 0.2 and 1.5 eV, with an average value of approximately 1.1 eV. These results imply that the onset of thermal excitation of electrons occurs between 53.8 and 67.8 GPa.

IV. CONCLUSIONS

Our DFT-MD simulations of water under shock loading show agreement with experimental results for shock Hugoniot pressures, temperatures, and densities. Our results provide validation of DFT with the generalized gradient approximation for the high pressure-temperature equation of state of water. At 42.0 GPa, we determine a progression from molecular H_2O to an ensemble of transient states of H^+, O^{2-}, OH^-, and H_2O, all which have lifetimes less than 50 fs. Determination of the chemical reactions in our simulations indicates that a unimolecular dissociation mechanism for ionic transport dominates along the shock Hugoniot and near the planetary isentrope. Lastly, at 67.8 GPa we predict large concentrations of negatively charged O and OH that contribute occupied electronic states near the band gap of the system. These species provide a simple mechanism for the transient metallization of water at higher pressures and temperatures.

ACKNOWLEDGMENTS

This work was performed under the auspices of the U.S. Department of Energy by Lawrence Livermore National Laboratory under Contract No. DE-AC52-07NA27344. Project No. 06-ERD-037 was funded by the Laboratory Directed Research and Development Program at LLNL. Computations were performed at LLNL using the following massively parallel computers: MCR, Thunder, uP, and Blue Gene L (BG/L). C.J.M. is supported by the U.S. Department of Energy's Office of Basic Energy Sciences, Chemical Sciences program at PNNL.

[1] K. K. M. Lee, L. R. Benedetti, R. Jeanloz, P. M. Celliers, J. H. Eggert, D. G. Hicks, S. J. Moon, A. Mackinnon, L. B. D. Silva, D. K. Bradley, W. Unites, and G. W. Collins, J. Chem. Phys. **125**, 014701 (2006).
[2] R. J. Hemley, A. P. Jephcoat, H. K. Mao, C. S. Zha, L. W. Finger, and D. E. Cox, Nature (London) **330**, 737 (1987).
[3] A. F. Goncharov, V. V. Struzkhin, M. S. Somayazulu, R. J. Hemley, and H. K. Mao, Science **273**, 218 (1996).
[4] F. Datchi, P. Loubeyre, and R. LeToullec, Phys. Rev. B **61**, 6535 (2000).
[5] J. F. Lin, B. Militzer, V. V. Struzkin, E. Gregoryanz, and R. J. Hemley, J. Chem. Phys. **121**, 8423 (2004).
[6] B. Schwager, L. Chudinovskikh, A. Gavriliuk, and R. Boehler, J. Phys.: Condens. Matter **16**, S1177 (2004).
[7] A. F. Goncharov, N. Goldman, L. E. Fried, J. C. Crowhurst, I.-F. W. Kuo, C. J. Mundy, and J. M. Zaug, Phys. Rev. Lett. **94**, 125508 (2005).
[8] Y. B. Zel'dovitch and Y. P. Raizer, *Physics of Shock Waves and High-Temperature Hydrodynamic Phenomena* (Dover, New York, 2002).
[9] S. T. Stewart and T. J. Ahrens, Geophys. Res. Lett. **30**, 1332 (2003).
[10] S. T. Stewart and T. J. Ahrens, J. Geophys. Res. **110**, E03005 (2005).
[11] S. T. Stewart and T. J. Ahrens, Geophys. Res. Lett. **35**, L23203 (2008).
[12] D. H. Dolan and Y. M. Gupta, J. Chem. Phys. **121**, 9050 (2004).
[13] D. H. Dolan, J. N. Johnson, and Y. M. Gupta, J. Chem. Phys. **123**, 064702 (2005).
[14] P. M. Celliers, G. W. Collins, D. G. Hicks, M. Koenig, E. Henry, A. Benuzzi-Mouniax, D. Batani, D. K. Bradley, L. B. DaSilva, R. J. Wallace, S. J. Moon, J. H. Eggert, K. K. M. Lee, L. R. Benedetti, R. Jeanloz, I. Masclet, N. Dague, B. Marchet, M. R. L. Gloahec, C. Reverdin, J. Pasley, O. Willi, D. Neely, and C. Danson, Phys. Plasmas **11**, L41 (2004).
[15] G. A. Lyzenga, T. J. Ahrens, W. J. Nellis, and A. C. Mitchell, J. Chem. Phys. **76**, 6282 (1982).
[16] J. D. Kress, S. R. Bickham, L. A. Collins, B. L. Holian, and S. Goedecker, Phys. Rev. Lett. **83**, 3896 (1999).
[17] A. Strachan, A. C. T. van Duin, D. Chakraborty, S. Dasgupta, and W. A. Goddard, Phys. Rev. Lett. **91**, 098301 (2003).
[18] E. J. Reed, M. R. Manaa, L. E. Fried, K. R. Glaesemann, and J. D. Joannopoulos, Nat. Phys. **4**, 72 (2008).
[19] N. C. Holmes, W. J. Nellis, W. B. Graham, and G. E. Walrafen, Phys. Rev. Lett. **55**, 2433 (1985).
[20] R. Chau, A. C. Mitchell, R. W. Minich, and W. J. Nellis, J. Chem. Phys. **114**, 1361 (2001).
[21] E. Schwegler, G. Galli, F. Gygi, and R. Q. Hood, Phys. Rev. Lett. **87**, 265501 (2001).
[22] K. Kadau, T. C. Germann, P. S. Lomdhal, and B. L. Holian, Science **296**, 1681 (2002).
[23] F. Gygi and G. Galli, Phys. Rev. B **65**, 220102 (2002).
[24] E. Schwegler, M. Sharma, F. Gygi, and G. Galli, Proc. Natl. Acad. Sci. U.S.A. **105**, 14779 (2008).
[25] M. Benoit, A. H. Romero, and D. Marx, Phys. Rev. Lett. **89**, 145501 (2002).
[26] A. Putrino and M. Parrinello, Phys. Rev. Lett. **88**, 176401 (2002).
[27] J. D. Kress, S. Mazevet, L. A. Collins, and W. W. Wood, Phys. Rev. B **63**, 024203 (2000).

[28] C. J. Mundy, A. Curioni, N. Goldman, I.-F. Kuo, E. Reed, L. E. Fried, and M. Ianuzzi, J. Chem. Phys. **128**, 184701 (2008).
[29] E. J. Reed, L. E. Fried, and J. D. Joannopoulos, Phys. Rev. Lett. **90**, 235503 (2003).
[30] E. Reed, L. E. Fried, M. R. Manaa, and J. D. Joannopoulos, in *Chemistry at Exteme Conditions*, edited by M. Manaa (Elsevier, Amsterdam, 2005).
[31] E. J. Reed, L. E. Fried, W. D. Henshaw, and C. M. Tarver, Phys. Rev. E **74**, 056706 (2006).
[32] R. Car and M. Parrinello, Phys. Rev. Lett. **55**, 2471 (1985); CPMD code, version 3.11.1, Copyright IBM Corp. 1990–2006, Copyright MPI für Festkörperforschung Stuttgart 1997–2001.
[33] A. D. Becke, Phys. Rev. A **38**, 3098 (1988).
[34] C. Lee, W. Yang, and R. G. Parr, Phys. Rev. B **37**, 785 (1988).
[35] J. P. Perdew, K. Burke, and M. Ernzerhof, Phys. Rev. Lett. **78**, 1396 (1997).
[36] R. Engelke, S. A. Sheffield, H. L. Stacy, and J. P. Quintana, Phys. Fluids **17**, 096102 (2005).
[37] J. M. Walsh and M. H. Rice, J. Chem. Phys. **26**, 815 (1957).
[38] A. C. Mitchell and W. J. Nellis, J. Chem. Phys. **76**, 6273 (1982).
[39] W. B. Hubbard, M. Podolak, and D. J. Stevenson, in *Neptune and Triton*, edited by D. P. Cruikshank (University of Arizona Press, Tucson, 1995).
[40] M. J. McGrath, J. I. Siepmann, I.-F. W. Kuo, C. J. Mundy, J. VandeVondele, J. Hutter, F. Mohamed, and M. Krack, ChemPhysChem **6**, 1894 (2005).
[41] N. Marzari and D. Vanderbilt, Phys. Rev. B **56**, 12847 (1997).
[42] N. Goldman, L. E. Fried, I.-F. W. Kuo, and C. J. Mundy, Phys. Rev. Lett. **94**, 217801 (2005).
[43] N. Goldman and L. E. Fried, J. Chem. Phys. **125**, 044501 (2006).
[44] N. Goldman and L. E. Fried, J. Chem. Phys. **126**, 134505 (2007).
[45] D. Chandler, J. Chem. Phys. **68**, 2959 (1978).
[46] D. A. McQuarrie, *Statistical Mechanics* (Harper, New York, 1976).
[47] R. S. Mulliken, J. Chem. Phys. **23**, 1833 (1955).
[48] CP2K code, http://www.cpk2.berlios.de (Copyright CP2K developers group 2000–2006); our calculations used the TZVP basis set for O and DZVP for H. The Goedecker–Teter–Hutter pseudopotential was used with a planewave cutoff of 280 Ry.
[49] C. Dellago, P. L. Geissler, D. Chandler, J. Hutter, and M. Parrinello, Phys. Rev. Lett. **89**, 199601 (2002).
[50] E. Schwegler, F. Gygi, G. Galli, and R. Q. Hood, Phys. Rev. Lett. **89**, 199602 (2002).
[51] S. Hamann and M. Linton, Trans. Faraday Soc. **62**, 2234 (1966).
[52] C. Cavazzoni, G. L. Chiarotti, S. Scandolo, E. Tosatti, M. Bernasconi, and M. Parrinello, Science **283**, 44 (1999).
[53] T. R. Mattsson and M. P. Desjarlais, Phys. Rev. Lett. **97**, 017801 (2006).
[54] P. Hunt, M. Sprik, and R. Vuilleumier, Chem. Phys. Lett. **376**, 68 (2003).
[55] G. Kresse and J. Hafner, Phys. Rev. B **47**, 558 (1993).